

Conduction pathways and mixed ionic-electronic conductivity below 500 °C in $\text{Ca}_x\text{Y}_{3-x}\text{Fe}_5\text{O}_{12-\delta}$ materials

Dnyaneshwar R. Bhosale^{1,2,3,*} and Shankar I. Patil^{2,†}

¹*Solid State Physics Division, Bhabha Atomic Research Centre, Mumbai 400085, India*

²*Department of Physics, Savitribai Phule Pune University, Pune 411007, India*

³*Department of Physics, Cummins College of Engineering for Women, Pune 411052, India*



(Received 19 April 2019; published 27 September 2019)

Mixed ionic-electronic conducting cathode material plays an important role in the operation of efficient low-temperature solid oxide fuel cells (LT-SOFCs). In the present study, we address the issue of achieving ionic conduction pathways and high mixed ionic-electronic conductivity below 500 °C in cathode materials for LT-SOFC technology. We report high mixed ionic-electronic conductivity in the low temperature range ($\sim 10^1 - 10^3 \text{ S cm}^{-1}$ at 350–500 °C) in the calcium-substituted yttrium iron garnets $\text{Ca}_x\text{Y}_{3-x}\text{Fe}_5\text{O}_{12-\delta}$ ($x = 0.15$). Oxide ion conduction is governed by an oxygen vacancy concentration mechanism presented here by soft bond valence sum distribution analysis of experimental neutron diffraction data up to 450 °C. The continuous minimum energy conduction pathways for oxide ions in the (100) plane have been visualized by soft bond valence sum analysis. The electronic conduction in present garnets occurs due to hopping of holes from Fe^{4+} to Fe^{3+} chemical states confirmed by Mössbauer spectroscopy. Importantly, the studied materials are found to be thermodynamically stable at least up to high temperatures of 800 °C, which supports well to frequent thermal cycles in SOFC devices. Another important parameter, viz. the thermal expansion coefficient, is found to be comparable with that for the conventionally used anode, electrolyte, and interconnect materials. On the basis of this study, we conclude that the present cathode materials would be useful for an efficient LT-SOFC technology.

DOI: [10.1103/PhysRevMaterials.3.095007](https://doi.org/10.1103/PhysRevMaterials.3.095007)

I. INTRODUCTION

Solid oxide fuel cells (SOFCs) are highly efficient, entirely ceramic fuel cells and a very important area of application for advanced ceramic materials in the energy sector [1–3]. On account of the superior advantages of SOFCs rather than commercially used battery power cells, there is research occurring in the materials society trying to develop more efficient SOFCs. The high performance of ceramic materials (cathode, anode, and electrolyte materials) is the most important aspect for the development of highly efficient, low-temperature SOFCs (LT-SOFCs, below 500 °C) [2]. High-temperature-operating (800–1100 °C) SOFCs have electrode-electrolyte incompatibility as well as sealing and thermodynamical instability issues which suppress the overall efficiency of the cell. Therefore, lowering the operating temperature is an important demand for the development of SOFC technology. The ceramic cathode, anode, and electrolyte materials in SOFC devices are mixed ionic-electronic, electronic, and pure ionic conductors, respectively. Research in SOFC technology has been focused for several decades on the advanced ceramic stable materials with their respective high conductivities (mixed, electronic and pure ionic for cathode, anode and electrolyte materials respectively) at low temperatures, below 500 °C, for high overall performance and high SOFC efficiency [1]. Many researchers have reported studies regarding the development

of cathode, anode, and electrolyte materials for SOFC technology [4–9]. Research on novel cathode materials includes work on Ba- and Sr-substituted LaMO_3 ($M = \text{Mn, Fe, Co, Ni}$) with mixed ionic-electronic conductivity, which are suitable for intermediate-temperature SOFCs (650–800 °C) [8,10–13]. The development of cathode materials in conventional SOFCs has mainly focused on the LaMO_3 system because this material remains stable in oxidizing atmospheres, has sufficient electrical conductivity ($\sim 150 - 1000 \text{ S cm}^{-1}$ at 1000 °C), depending on the substituent, and has a close thermal expansion match to the conventional electrolyte yttria-stabilized zirconia (YSZ) [14]. But it has several unresolved issues in order to have acceptable performance at low-temperature operations below 500 °C [15]. In view of this, there remains a strong motivation to search for improved stable cathode materials with high mixed ionic-electronic conductivity at temperatures below 500 °C.

In recent years it was found that divalent substituted iron garnets are promising cathode materials with sufficient mixed conductivity for intermediate-temperature SOFC operation (650–800 °C) [16,17]. But the divalent substituted iron garnets suffer from the unavailability of adequate transport pathways in the crystal lattice for ionic conduction. Low values of mixed ionic-electronic conductivity ($\sim 1 - 10 \text{ S cm}^{-1}$ at 500 °C) for various divalent substituted iron garnet compounds have been reported [16,17]. The low conductivity is due to the heavy substitution of Ca^{2+} ion (100 pm) at the Y^{3+} ion (90 pm) site [17]. A heavy substitution of Ca^{2+} ion at the Y^{3+} ion site reduces the oxide ion transport pathways, resulting in low overall electrical conductivity [16]. Moreover, heavy

*Corresponding author: drbhosale@physics.unipune.ac.in

†Corresponding author: patil@physics.unipune.ac.in

substitution ($x \geq 0.2$) results in secondary perovskite phase formation, which is also responsible for low mixed ionic-electronic conduction [18]. The mixed ionic-electronic conductivity of oxide ions has been reported for $\text{Gd}_{3-x}\text{A}_x\text{Fe}_5\text{O}_{12\pm\delta}$ ($A = \text{Ca}$; $x = 0-0.8$) and $\text{Y}_{3-x-y}\text{Ca}_x\text{Nd}_y\text{Fe}_{5-z}\text{Ni}_z\text{O}_{12-\delta}$ ($x = 0-0.5$; $y = 0-0.25$; and $z = 0-1.0$) garnets [16]. However, the observed mixed conductivity in these garnets is quite low, even at high temperatures ($\sim 10 \text{ S cm}^{-1}$ at $\sim 800^\circ\text{C}$), mainly due to the unavailability of suitable easy oxide ion transport (conduction) pathways [19]. Oxide ion conductivity depends upon the availability of facile oxide ion conduction pathways and the concentration of vacancies of oxygen ions in the lattice. The lower ionic transport in garnets reported in literature suffers from the unavailability of sufficient conduction pathways and low oxygen ion vacancy concentration. In this regard, materials engineering plays a vital role. Here in the present research work, we tackle this issue. In the present work, on account of materials engineering we have optimized the divalent substituent content to afford high electronic as well as oxide ion conduction. Moreover, in the present study, a judicious choice of substitution (small size electropositive Y^{3+} ions are replaced by an appropriate content of larger size high electropositive divalent Ca^{2+} ions) affords minimum energy pathways for oxide ion conduction and sufficient vacancies of oxide ions. The present work reveals high oxide ion conduction through the various polyhedral networks (tetrahedron: $\text{FeO}_4 \rightarrow$ octahedron: $\text{FeO}_6 \rightarrow$ dodecahedron: Ca/YO_8) in the studied iron garnets, even at low temperatures of around 450°C .

In the present study, we report an high mixed ionic-electronic conductivity $\sim 10^1-10^3 \text{ S cm}^{-1}$ at close to room temperature range $350-500^\circ\text{C}$ in Ca-substituted yttrium iron garnet $\text{Ca}_x\text{Y}_{3-x}\text{Fe}_5\text{O}_{12-\delta}$ ($x = 0.15$) cathode material. The electronic conduction mechanism is based on the hopping of holes from Fe^{4+} to Fe^{3+} ions in the present iron garnet compounds. The substitution of high electropositive divalent ion (Ca^{2+}) at the Y^{3+} ion site affords high mixed ionic-electronic conductivity at a very low temperature range ($350-500^\circ\text{C}$). The oxide ion conductivity in the present materials is well understood on the basis of continuous minimum energy pathways for oxide ion conduction at low temperature (450°C). The conduction pathways for oxide ions in iron garnets are revealed by neutron diffraction studies at various temperatures up to 450°C . Our study further reveals the thermal expansion compatibility and high thermodynamical stability of the present Ca-substituted iron garnets, which is also a major outlook in the development of cathode materials for low-temperature SOFC technology.

II. EXPERIMENTAL

The powder samples of $\text{Ca}_x\text{Y}_{3-x}\text{Fe}_5\text{O}_{12-\delta}$ ($x = 0, 0.06, 0.15, \text{ and } 0.2$) were synthesized by conventional ceramic methods by reacting high-purity (99.9%) CaCO_3 , Y_2O_3 , and Fe_2O_3 oxides (Sigma Aldrich) in the $x:3-x:5$ proportions at high temperature. The homogeneous mixtures of CaCO_3 , Y_2O_3 , and Fe_2O_3 were obtained by dry and wet grinding of CaCO_3 , Y_2O_3 , and Fe_2O_3 oxides with isopropyl alcohol. The two-step calcinations of the mixture were done at 950°C

and 1050°C in air using a high-temperature furnace with three intermediate grindings. The final mixture was sintered in a platinum crucible at 1200°C for 20 h and then cooled slowly to room temperature at a rate of $1^\circ\text{C}/\text{min}$. Powder samples were pelletized in rectangular bars by applying a pressure of 2.5 ton using a hydraulic press and then fired at 1200°C (similar to annealing temperature) in air atmosphere. The prepared bar samples of size ($\sim 10 \times 5 \times 2 \text{ mm}$) were used for conductivity measurements. The x-ray diffraction (XRD) measurements were performed on the powder samples of $\text{Ca}_x\text{Y}_{3-x}\text{Fe}_5\text{O}_{12-\delta}$ ($x = 0, 0.06, 0.15, \text{ and } 0.2$) at room temperature (RT) in a Bragg-Brentano geometry using a $\text{Cu } K\alpha_1$ radiation on a Rigaku diffractometer. The measured XRD patterns were analyzed by the Rietveld refinement method. The thermogravimetric and differential scanning calorimetric measurements were simultaneously performed on the powder samples in air atmosphere with $10^\circ\text{C}/\text{min}$ heating rate using a Linseis instrument. The high-temperature conductivity measurements (in air atmosphere) were carried out on the bar samples ($10 \times 5 \times 2 \text{ mm}$) using a four-probe method. Neutron diffraction experiments over $27-450^\circ\text{C}$ were performed using the powder diffractometer II ($\lambda = 1.2443 \text{ \AA}$) at the Dhruva reactor (Trombay, Mumbai, India). For recording neutron diffraction patterns, a powder sample ($\sim 8 \text{ gm}$) was placed in a cylindrical vanadium container under vacuum ($\sim 10^{-5}$ torr) and patterns were recorded with five position-sensitive detector based powder diffractometer covering a Q ($4\pi \sin \theta/\lambda$, where 2θ is the scattering angle and λ is the neutron wavelength)-range of $0.53-9.398 \text{ \AA}^{-1}$. The collected neutron diffraction data were analyzed by the Rietveld refinement method as well as the soft bond valence method utilizing the FULLPROF software suite [20]. The oxide ion conduction pathways (obtained by combination of the Rietveld and the soft bond valence methods) were analyzed and visualized using the computer program VESTA [21]. The dc magnetization measurements were carried out using a vibrating sample magnetometer as a function of both temperature (T) and magnetic field (H). The temperature-dependent magnetization measurements were carried out under field-cooled (FC) conditions. For the FC measurements, the sample was cooled from room temperature down to the lowest temperature of 5 K in the presence of applied magnetic field (200 Oe), and the magnetization was measured in the warming cycle under the same field over temperatures of $27-310^\circ\text{C}$. Magnetization vs magnetic field curves was recorded at -268°C over a $\pm 50 \text{ kOe}$ magnetic field. Mössbauer spectrums of present iron garnets at room temperature were recorded using a Mössbauer spectrometer operated in constant acceleration mode in transmission geometry. The isomer shift (δ) values were derived relative to Fe metal foil ($\delta = 0.0 \text{ mm/s}$) to know the oxidation state of the Fe ions.

III. RESULTS AND DISCUSSION

The prepared samples are well characterized with x-ray and neutron diffraction (described later) and Mössbauer spectroscopy techniques which confirm the structural and magnetic properties of iron garnets (Supplemental Material Figs. S1-S4) [22]. The Rietveld refined XRD profiles in

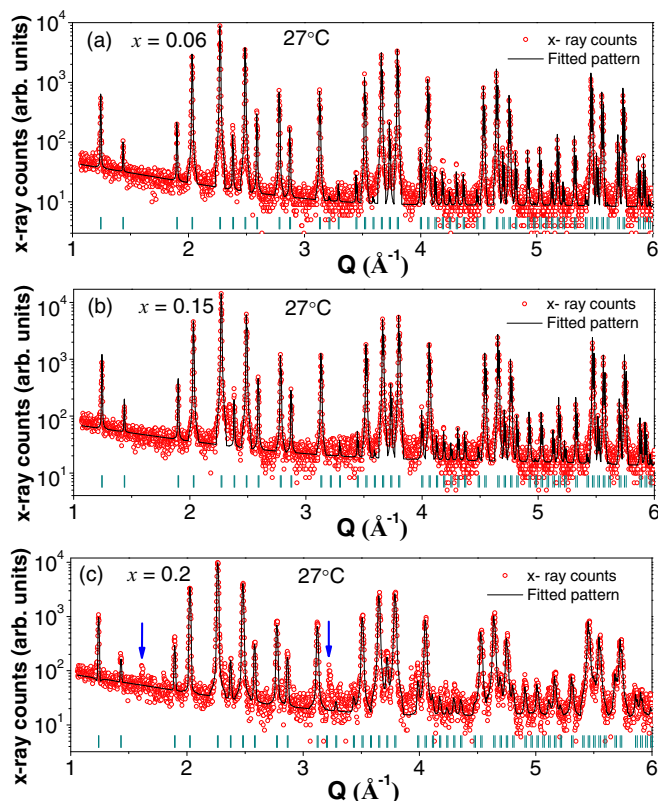


FIG. 1. Rietveld refined x-ray diffraction profiles in logarithmic scale (y axis) for $\text{Ca}_x\text{Y}_{3-x}\text{Fe}_5\text{O}_{12-\delta}$ ($x = 0.06, 0.15,$ and 0.2) compounds. Observed data are shown as open circles, and the Rietveld calculated patterns are shown as solid lines. The short vertical bars indicate the position of allowed Bragg peaks. Arrows in (c) show the x-ray intensity coming from impurity perovskite $(\text{Ca}/\text{Y})\text{FeO}_3$ phase.

logarithmic scale (y axis) as shown in Fig. 1 clearly show the pure iron garnet cubic phase for $x = 0.06$ and 0.15 compounds, whereas the $x = 0.2$ compound gives an additional unwanted “perovskite impurity phase” as marked by arrows in Fig. 1(c). All the studied iron garnets ($x = 0, 0.06,$ and 0.15) possess a bcc structure with $Ia-3d$ space group. There are eight formula units in the unit cell of iron garnets $\text{Ca}_x\text{Y}_{3-x}\text{Fe}_5\text{O}_{12-\delta}$. The $\text{Y}^{3+}/\text{Ca}^{3+}$ ions occupy the center of eight cornered 12-sided, dodecahedron (24c) Wyckoff positions, whereas Fe^{3+} ions occupy the centers of tetrahedron (24d) and octahedron (16a) Wyckoff positions, and oxygen ions occupy the general (96h) positions. Figure 2(a) shows the results of dc magnetization measurements with temperature. Magnetization measurements have revealed the Curie temperatures for both the substituted compounds in the range 280–300 °C. Neutron diffraction patterns for the $x = 0.15$ compound at various temperatures over 27–450 °C reveal a ferrimagnetic-to-paramagnetic transition around the similar range, 280–300 °C [Fig. 2(b)]. Figure 3(a) shows the variation of mixed conductivity with temperature for all prepared compositions. The required high mixed ionic-electronic conductivity $1.11 \times 10^3 \text{ S cm}^{-1}$ is observed at 500 °C for $\text{Ca}_{0.15}\text{Y}_{2.85}\text{Fe}_5\text{O}_{12-\delta}$ compound. A ferrimagnetic-to-paramagnetic transition at around 280–300 °C in conductivity data is well reflected, in agreement with the dc

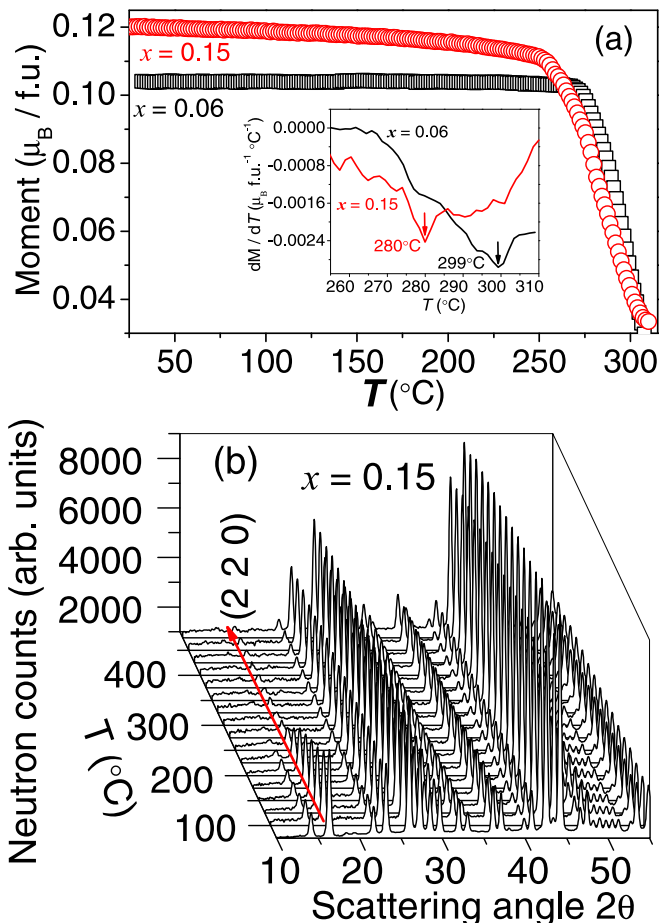


FIG. 2. (a) The variation of magnetization (moment, M) with temperature under the magnetic field of 200 Oe. Inset shows the variation of dM/dT with temperature reveals the ferrimagnetic-to-paramagnetic transition temperatures. (b) Experimental neutron diffraction profiles for the $x = 0.15$ compound at various temperatures over 27–450 °C. The various profiles for the $x = 0.15$ compound showing the variation of integrated intensity of the (220) magnetic peak with temperature, revealing a ferrimagnetic-to-paramagnetic transition around the same temperature (300 °C).

magnetization and neutron diffraction data. An Arrhenius plot of mixed conductivity $[\ln(\sigma T) = \ln(A) - E_a/RT]$, where σ is conductivity, T is temperature, E_a is activation energy, A is the preexponential factor, and R is the universal gas constant] above the ferrimagnetic-to-paramagnetic transition temperature is shown in Fig. 3(b) for all prepared compositions. The activation energies for the present compounds (~ 0.3 – 0.7 eV) are found to be less compared to the reported values of iron garnets as mixed conductors [16]. The derived high value of the preexponential factor ($\ln A = 28.007(2)$ for $x = 0.15$), related to the diffusion coefficient parameter, results in a high mixed conductivity [23].

The mechanism of electronic conduction in divalent substituted iron garnets such as $\text{Y}_{3-2x}\text{Ca}_{2x}\text{Fe}_{5-x}\text{V}_x\text{O}_{12}$ ($0.0 \leq x \leq 0.6$) is reported in literature [24]. Electronic conduction in the present compounds is due to hopping of holes from Fe^{4+} to Fe^{3+} ions. The presence of an Fe^{4+} chemical state in $\text{Ca}_x\text{Y}_{3-x}\text{Fe}_5\text{O}_{12-\delta}$, unlike the parent yttrium iron garnet,

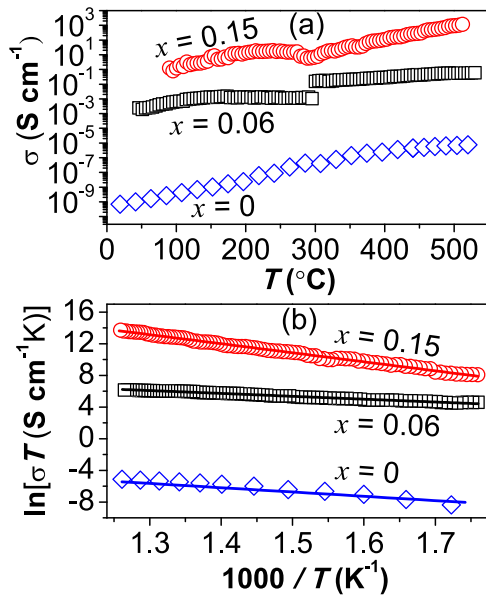


FIG. 3. (a) Variation of mixed ionic-electronic conductivity with temperature for Ca-substituted iron garnets. (b) Arrhenius plot of mixed ionic-electronic conductivity above the ferrimagnetic-to-paramagnetic transition temperature for the same iron garnet samples. For comparison, conductivity plots for the parent YIG compound are also included.

$\text{Y}_3\text{Fe}_5\text{O}_{12}$ (YIG), is because of divalent calcium ion (Ca^{2+}) substitution at the trivalent yttrium ion (Y^{3+}) site (24c). The presence of Fe ion in 4+ chemical states in both the substituted compounds has been revealed here by Mössbauer spectroscopy measurements. The isomer shift values, $\delta = 0.132 \pm 0.002$ and $\delta = 0.354 \pm 0.002$, confirm the oxidation state “4+” of Fe ion at tetrahedral site (24d) and “3+” of Fe ion at octahedral site (16a), respectively, for the $x = 0.15$ compound. Similar results are found for the other $x = 0.06$ compound, whereas for the parent YIG compound both sites (tetrahedral and octahedral) of Fe ions are in the “+3” oxidation state (Supplemental Material Table S1 [22]). We note here that the transportation of oxide ions in parent YIG compound occurs only at high temperatures above 900 °C [16]. An electronic conductivity of $\sim 10^{-5} \text{ S cm}^{-1}$ at 500 °C for the parent YIG compound is well reported in the literature, which is found to be in agreement with our results for YIG compound [24]. We note that ceramic microstructures do not play any significant role in altering the ionic conductivity of such iron garnets (i.e., no grain boundary effect, unlike in perovskite materials [16]), as similar values of ionic diffusivities are reported in single-crystalline and polycrystalline $\text{Y}_3\text{Fe}_5\text{O}_{12}$ [25].

In order to understand the oxide ion conduction mechanism, we have performed neutron diffraction experiments at various temperatures over 27–450 °C for all prepared compounds [Fig. 2(b)]. Rietveld refined neutron diffraction profiles for substituted compounds at 27 and 450 °C are shown in Fig. 4. By using experimental neutron diffraction data, we have traced the ionic conduction pathways in crystal lattices by employing the popular soft bond valence

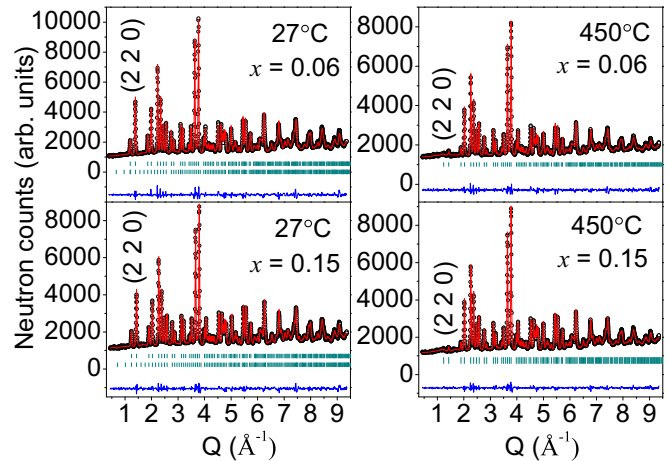


FIG. 4. Rietveld refined neutron diffraction profiles at 27 and 450 °C for $x = 0.06$ and 0.15 compounds. Experimental profiles and calculated patterns are shown by open circles and a solid line, respectively. The difference between the experimental profiles and calculated patterns is also shown by a solid line at the bottom of each panel. The short vertical bars indicate the positions of allowed nuclear Bragg peaks for the crystalline phase. The magnetic Bragg peaks are marked at the bottom by nuclear Bragg peak markers for profiles at 27 °C. The intense magnetic peaks (2 2 0) are missing for both compounds ($x = 0.06$ and 0.15) in the paramagnetic state at 450 °C.

method technique [26]. The structural parameters (Table I and Supplemental Material S2(d–h) [22]) derived from the Rietveld refinement of neutron diffraction patterns were used in the soft bond valence method to obtain the isosurfaces of the soft bond valence sum distribution with constant bond valence mismatch of 0.2 valence units (v.u.). Isosurfaces of bond valence sum distribution in three dimensions (3D) representing the oxide ion most probable conduction pathways for both compounds are shown in Figs. 5(a) and 5(b). The most probable pathways in 3D reveal the facile oxide ion conduction through the various polyhedral networks as per the order $[\text{Ca}/\text{YO}_7][\text{FeO}_6][\text{FeO}_4] \rightarrow [\text{Ca}/\text{YO}_8][\text{FeO}_5][\text{FeO}_4] \rightarrow [\text{Ca}/\text{YO}_8][\text{FeO}_6][\text{FeO}_3]$ in the studied iron garnets based on the oxygen vacancy concentration mechanism. Importantly, we could admirably trace the paths based on the oxide ion vacancy concentration mechanism for conduction at low temperatures around 450 °C by employing experimental neutron diffraction data (Fig. 5).

TABLE I. The structural parameters derived from refinement of the neutron diffraction patterns for $x = 0.15$, at 450 °C. X, Y, Z: positions; OCC: occupancy.

Ions (site)	X	Y	Z	OCC
Y (24c)	0	1/4	1/8	0.95
Fe ₁ (16a)	0	0	0	1
Fe ₂ (24d)	0	1/4	3/8	1
Ca (24c)	0	1/4	1/8	0.05
O (96h)	−0.0267 (1)	0.0566 (1)	0.1515 (2)	0.960 (4)

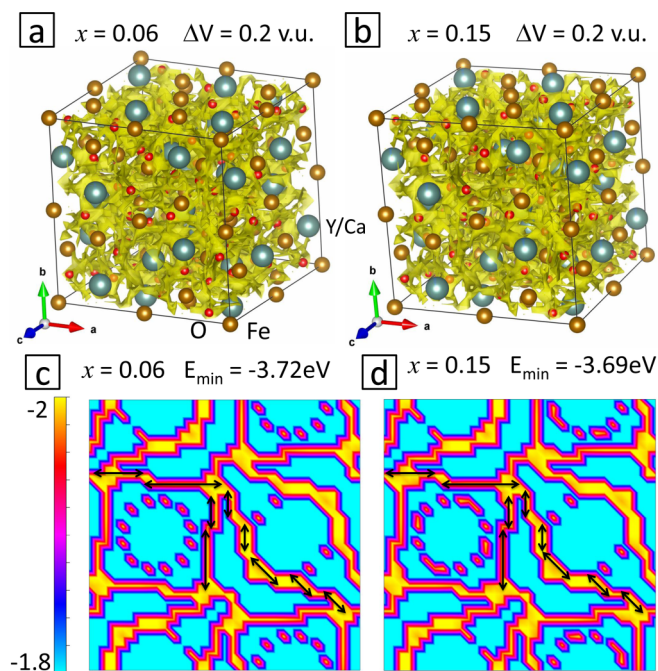


FIG. 5. Visualization of oxide ion conduction pathways at 450 °C in the unit cells of the present iron garnet crystal by employing the soft bond valence method on experimental neutron diffraction data. Isosurfaces of the bond valence sum distribution with the atomic model in 3D for $x =$ (a) 0.06 and (b) 0.15 compounds show the most probable ionic conduction pathways along various polyhedra. The minimum energy oxide ion conduction pathways in the (100) crystal plane for $x =$ (c) 0.06 and (d) 0.15 compounds are shown. Isosurfaces of soft bond valence sum distribution were obtained with bond valence mismatch $\Delta V = 0.2$ v.u. Arrows in (c) and (d) show the directions of oxide ion conduction, which depends on the gradient of oxygen chemical potential. The background color of the planar image corresponds to lowest value of the soft bond valence sum in valence units.

Bond valence sum distribution maps can be correlated to the energy scale of bond valence mismatch (valence unit to electron volt) by employing the Morse potential [27,28]. Based on soft bond valence sum distribution for the substituted compounds, the minimum energy (corresponding to chemical state -2) oxide ion conduction pathways in the (100) plane have been traced as shown in Figs. 5(c) and 5(d). Arrows marked in the planer view of minimum energy conduction pathways represent the direction of oxide ion conduction under the gradient of oxygen chemical potential [16]. We note here that the observed high electrical conductivity ($\sim 10^1 - 10^3$ S cm $^{-1}$ at 350–500 °C) is on account of such facile oxide ion conduction pathways at close to RT, around 350–450 °C. Similar oxide ion conduction pathways (Fig. 5) are found to be observed at 800 °C, except the volume for oxide ion transport in the unit cell is substantial. Based on soft bond valence sum distribution analysis at various temperatures over 27–450 °C, we have estimated the oxide ion minimum energy over 27–450 °C by linking bond valence mismatch to the energy scale for both the compounds. Figure 6(a) shows the variation of minimum energy for oxide ions with temperature. A systematic increase in values of

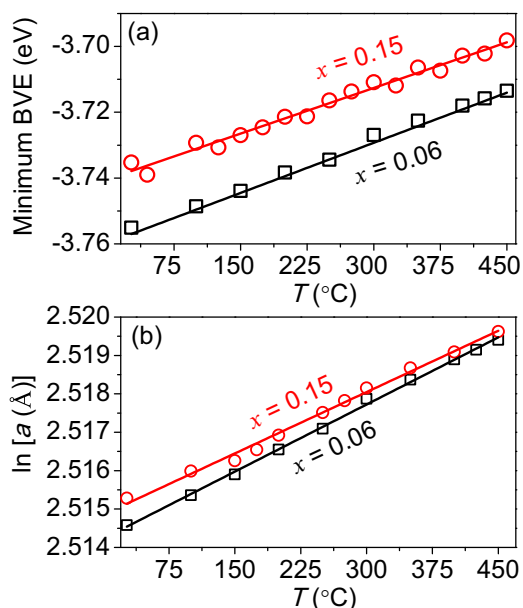


FIG. 6. (a) The variation of minimum bond valence energy of oxide ions with temperature for the substituted compounds. The minimum bond valence energy is obtained by linking the soft bond valence mismatch with Morse potential. (b) Variation of the natural logarithm of the lattice constant with temperature (derived from the Rietveld analysis of experimental neutron diffraction profiles) for the substituted compounds. Error bars for both plots is in the symbols.

minimum energy with temperature for substituted compounds clearly represents the participation of oxide ions in the conduction process by losing its stability. The variation of the natural logarithm of the lattice constant with temperature [Fig. 6(b)] shows that the linear thermal expansion provides enough volume for oxide ion conduction through various polyhedral networks in the substituted compounds. As described earlier, the conduction of oxide ions through various polyhedral networks in the present iron garnet compounds is based on the vacancy concentration mechanism [16]. In the present study, we have quantified the vacancy concentration for both the substituted compounds from the thermogravimetric analysis and from neutron diffraction data. The temperature variation of the oxygen content ($12 - \delta$) shows an increase in the oxygen vacancy concentration with increasing temperature [Fig. 7(a)]. Oxide ion occupancy of 96% for $x = 0.15$ at 450 °C derived from refinement of neutron diffraction data further reveals the oxygen vacancy concentration in both substituted compounds (Table I and Supplemental Material S2(d–h) [22]).

Now we discuss the thermodynamical stability of the present cathode material over the extended range of temperature up to 800 °C for SOFC operation. The present study is based on the iron garnets, which are generally known for their high structural stability up to a very high temperature range of 1100–1400 °C. Geller *et al.* have shown that there is no change in structural symmetry for YIG up to 900 °C [29]. The stability of Ca-substituted iron garnets, $Y_{3-x}Ca_xFe_5O_{12-\delta}$, is even confirmed in the reducing H_2/H_2O atmosphere of the anode at temperatures up to 650 °C in a SOFC device [17]. Further, the $Y_{3-x}Ca_xFe_5O_{12-\delta}$ and $Gd_{3-x}Ca_xFe_5O_{12-\delta}$

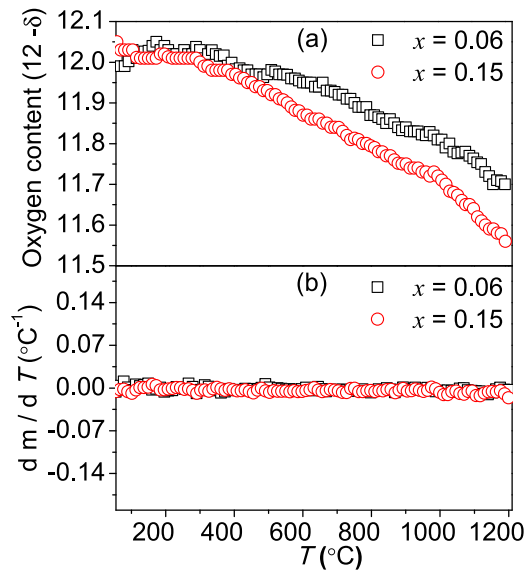


FIG. 7. (a) Variation of oxygen content with temperature for the ($x = 0.06$ and 0.15) substituted compositions. (b) Differential thermal curves for the substituted compounds up to 1200 °C. Differential thermal curves do not show any structural phase transition at least up to 1200 °C for both the compounds.

garnets are reported to be stable at least up to 1000 °C in an oxygen partial pressure gradient [16]. Our differential thermal analysis [Fig. 7(b)] and neutron diffraction profiles at 800 °C [Figs. 8(a) and 8(b)] confirm the thermal stability of both compounds at least up to 800 °C in air atmosphere. Time differential relative mass analysis shown in Figs. 8(c) and 8(d) for both compounds reveals that the present iron

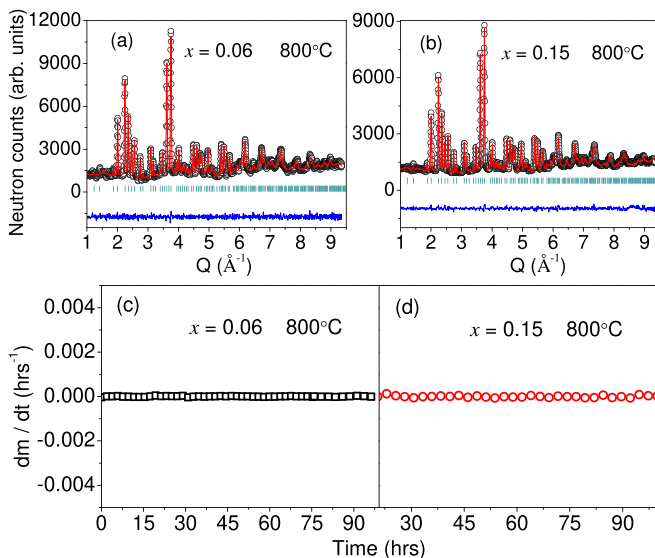


FIG. 8. (a, b) Rietveld refined neutron diffraction profiles showing the studied compositions retain the same bcc phase of iron garnets even at 800 °C. (c, d) Time differential of relative mass m at constant temperature of 800 °C for 100 h under air atmosphere using the thermogravimetric analysis (TGA) instrument reveals no decomposition or phase transition with time (free from aging effects) for the substituted samples.

garnets are free from the aging effects. We note here that attempts were made to synthesize $Y_{3-x}Ca_xFe_5O_{12-\delta}$ with $x \geq 0.2$, but this resulted in a secondary unwanted perovskite phase $(Y/Ca)FeO_3$, as revealed by Rietveld analysis of the XRD profile for the $x = 0.2$ composition [see Figs. 1(c) and Supplemental Material S3] [22]. This reduces the ionic-electronic transport properties beyond $x \geq 0.2$ for the present garnet compounds [16,17].

Another important parameter for SOFC operation is the thermal expansion coefficient (TEC) of electrode-electrolyte materials used in SOFC devices. In the present study we have derived TECs of $11.65 \times 10^{-6}/^\circ\text{C}$ for $x = 0.06$ and $10.64 \times 10^{-6}/^\circ\text{C}$ for $x = 0.15$ compound by fitting a straight line to the temperature dependence of the natural logarithm of the lattice constant over 27 – 450 °C (derived from neutron diffraction study) as shown in Fig. 6(b). A similar range of TEC values has been reported for various iron garnets in the literature [16]. The derived values of TEC of the present garnets are found to be closer to those of the anode, electrolyte, and interconnect materials used in conventional SOFC devices, making the present garnets suitable as cathode materials for use in LT-SOFC devices.

IV. CONCLUSIONS

In conclusion, a high mixed ionic-electronic conductivity ($\sim 10^1$ – 10^3 S cm^{-1} at 350 – 500 °C), an important need for the development of LT-SOFC technology, is revealed in cathode materials $Ca_xY_{3-x}Fe_5O_{12-\delta}$ ($x = 0.15$). An oxygen vacancy concentration mechanism has been revealed by the soft bond valence sum distribution analysis of neutron diffraction data. Minimum energy pathways have been visualized in the (100) plane for easy oxide ion conduction at low temperatures (450 °C). An electronic conduction mechanism based on hopping of holes from Fe^{4+} to Fe^{3+} in the present iron garnet compounds has been revealed. An important issue of the thermal stability of the present cathode materials up to high temperature (800 °C) for supporting frequent cycles in SOFC devices has been addressed. The thermal expansion compatibility of the studied iron garnet cathode materials has been confirmed with commonly used anode, electrolyte, and interconnect materials used in conventional SOFC devices. Our finding of high mixed ionic-electronic conductivity at relatively low temperature makes the present thermally stable garnet compound $Ca_xY_{3-x}Fe_5O_{12-\delta}$ ($x = 0.15$) a promising cathode material for the development of LT-SOFC technology.

ACKNOWLEDGMENTS

The present work has been carried out under the BARC (Mumbai)–SPPU (Pune) collaborative research scheme by D.B. D.B. is grateful to S. M. Yusuf for his encouragement and support in this work. D.B. would like to thank R. Godbole and S. Bhagwat for their help in the conductivity measurement experiments and is also grateful to A. Shinde and P. S. R. Krishna for their help during the neutron diffraction experiments. D.B. acknowledges the help provided by P. Bhatt during the thermogravimetric and differential scanning calorimetric measurements and strongly acknowledges the help provided by Sher Singh Meena for Mössbauer spectroscopy measurements.

- [1] E. D. Wachsman and K. T. Lee, *Science* **334**, 935 (2011).
- [2] E. Wachsman, T. Ishihara, and J. Kilner, *MRS Bull.* **39**, 773 (2014).
- [3] R. M. Ormerod, *Chem. Soc. Rev.* **32**, 17 (2003).
- [4] Z. Shao and S. M. Haile, *Nature (London)* **431**, 170 (2004).
- [5] T. Hibino, A. Hashimoto, M. Yano, M. Suzuki, S.-i. Yoshida, and M. Sano, *J. Electrochem. Soc.* **149**, A133 (2002).
- [6] S. J. Skinner and J. A. Kilner, *Mater. Today* **6**, 30 (2003).
- [7] C. Xia, W. Rauch, F. Chen, and M. Liu, *Solid State Ionics* **149**, 11 (2002).
- [8] J. Molenda, K. Świerczek, and W. Zając, *J. Power Sources* **173**, 657 (2007).
- [9] J. M. Ralph, C. Rossignol, and R. Kumar, *J. Electrochem. Soc.* **150**, A1518 (2003).
- [10] K. Świerczek, J. Marzec, D. Pałubiak, W. Zając, and J. Molenda, *Solid State Ionics* **177**, 1811 (2006).
- [11] K. Świerczek and M. Gozu, *J. Power Sources* **173**, 695 (2007).
- [12] K. Świerczek, *Solid State Ionics* **179**, 126 (2008).
- [13] J. Molenda, J. Kupecki, R. Baron, M. Blesznowski, G. Brus, T. Brylewski, M. Bucko, J. Chmielowiec, K. Cwieka, M. Gazda, A. Gil, P. Jasinski, Z. Jaworski, J. Karczewski, M. Kawalec, R. Kluczowski, M. Krauz, F. Krok, B. Lukasik, M. Malys *et al.*, *Int. J. Hydrogen Energy* **42**, 4366 (2017).
- [14] K. Huang, M. Feng, J. B. Goodenough, and M. Schmerling, *J. Electrochem. Soc.* **143**, 3630 (1996).
- [15] J. Ralph, A. Schoeler, and M. Krumpelt, *J. Mater. Sci.* **36**, 1161 (2001).
- [16] V. Kharton, A. Shaula, E. Naumovich, N. Vyshatko, I. Marozau, A. Viskup, and F. Marques, *J. Electrochem. Soc.* **150**, J33 (2003).
- [17] W. Zhong, Y. Ling, Y. Rao, R. Peng, and Y. Lu, *J. Power Sources* **213**, 140 (2012).
- [18] S. Geller and M. Gilleo, *J. Phys. Chem. Solids* **3**, 30 (1957).
- [19] D. R. Bhosale, S. M. Yusuf, A. Kumar, M. D. Mukadam, and S. I. Patil, *Phys. Rev. Mater.* **1**, 015001 (2017).
- [20] J. Rodriguez-Carvajal, PROGRAM FullProf.2k (Version 5.80 - May2016-ILL JRC).
- [21] K. Momma and F. Izumi, *J. Appl. Crystallogr.* **44**, 1272 (2011).
- [22] See Supplemental Material at <http://link.aps.org/supplemental/10.1103/PhysRevMaterials.3.095007> for $\text{Ca}_x\text{Y}_{3-x}\text{Fe}_5\text{O}_{12}$.
- [23] Y. Teraoka, H. Zhang, K. Okamoto, and N. Yamazoe, *Mater. Res. Bull.* **23**, 51 (1988).
- [24] A. A. El Ata, N. Sharaf, M. Ahmed, and B. Shalaby, *Solid State Sci.* **6**, 639 (2004).
- [25] A. E. Paladino, E. A. Maguire Jr., and L. G. Rubin, *J. Am. Ceram. Soc.* **47**, 280 (1964).
- [26] I. D. Brown, *Chem. Rev.* **109**, 6858 (2009).
- [27] M. Monchak, T. Hupfer, A. Senyshyn, H. Boysen, D. Chernyshov, T. Hansen, K. Schell, E. Bucharsky, M. Hoffmann, and H. Ehrenberg, *Inorg. Chem.* **55**, 2941 (2016).
- [28] S. Adams and R. P. Rao, *Phys. Status Solidi A* **208**, 1746 (2011).
- [29] S. Geller, H. J. Williams, R. C. Sherwood, J. P. Remeika, and G. P. Espinosa, *Phys. Rev.* **131**, 1080 (1963).